BIOCHEMISTRY
including biophysical chemistry & molecular biology

Article

pubs.acs.org/biochemistry

Structural Investigations into the Stereochemistry and Activity of a Phenylalanine-2,3-aminomutase from *Taxus chinensis*

Gjalt G. Wybenga,[†] Wiktor Szymanski,[‡,§] Bian Wu,[‡] Ben L. Feringa,[§] Dick B. Janssen,[‡] and Bauke W. Dijkstra*[,†]

[†]Laboratory of Biophysical Chemistry, University of Groningen, Nijenborgh 7, 9747 AG Groningen, The Netherlands

[‡]Department of Biochemistry and [§]Center for Systems Chemistry, University of Groningen, Nijenborgh 4, 9747 AG Groningen, The Netherlands

Supporting Information

ABSTRACT: Phenylalanine-2,3-aminomutase (PAM) from *Taxus chinensis*, a 4-methylidene-imidazole-5-one (MIO)-dependent enzyme, catalyzes the reversible conversion of (*S*)-α-phenylalanine into (*R*)-β-phenylalanine via *trans*-cinnamic acid. The enzyme also catalyzes the direct addition of ammonia to *trans*-cinnamic acid, a reaction that can be used for the preparation of β-amino acids, which occur as frequent constituents of bioactive compounds. Different hypotheses have been formulated to explain the stereochemistry of the PAM-catalyzed reaction, but structural evidence for these hypotheses is lacking. Furthermore, it remains unclear how the PAM MIO group is formed from the three-amino acid (A-S-G) sequence motif. For these reasons, we elucidated PAM three-dimensional (3D) structures with a bound (*R*)-β-phenylalanine analogue and with bound *trans*-cinnamic acid. In addition, 3D structures of the (inactive) Y322A and N231A mutants of PAM were elucidated, which were found to be MIO-less. We conclude that the stereochemistry of the PAM-catalyzed reaction originates from the enzyme's ability to bind *trans*-cinnamic acid in two different orientations, with either the *si*,*si* face or the *re*,*re* face directed toward the MIO group, as evidenced by two distinct carboxylate binding modes. The results also suggest that the N231 side chain promotes MIO group formation by increasing the nucleophilicity of the G177 N atom through acidification of the amide proton.

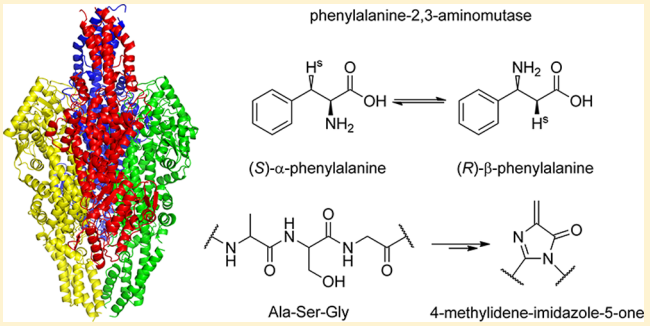

The development of methods for the synthesis of β-amino acids has attracted considerable attention because of the interesting biological activities of various compounds in which they are present.[1,2] Many β-amino acid-containing bioactive compounds isolated from plants and microorganisms have been described, of which Taxol [paclitaxel, **1** (Figure 1A)], obtained from *Taxus brevifolia* by Wani et al.,[3] is a notable example. Taxol is an effective antitumor drug[4] for which there is strong demand. However, the natural supply of Taxol is limited because *Taxus* sp. are slow-growing and produce only small quantities of the compound.[5] Total synthesis of Taxol has been demonstrated but is not efficient.[6−8] Semisynthesis using more readily available *Taxus* metabolites is feasible, but starting materials still need to be harvested from the trees.[9] Synthesis of Taxol via a biosynthetic pathway is therefore considered to be of paramount importance for the wider application of this compound.[10]

An important step in the production of Taxol is the synthesis of the *N*-benzoyl-phenyl-isoserinoyl side chain, which is essential for biological activity.[11] This side chain is synthesized from (*R*)-β-phenylalanine [(*R*)-β-Phe, **2** (Figure 1B)],[12] which, in *Taxus* sp., is made from (*S*)-α-phenylalanine [(*S*)-α-Phe, **4** (Figure 1B)] by the action of phenylalanine-2,3-aminomutase (PAM).[13,14] PAM also catalyzes the reverse reaction and can be utilized for the synthesis of enantiopure aromatic β-amino acids by either the isomerization of α-amino acids[15] or the amination of *trans*-cinnamic acid [*t*-CA, **3** (Figure 1B)] and its ring-substituted derivatives.[16,17]

PAMs from three different sources have been characterized. PAM from *Taxus chinensis* (PAM) is a tetrameric protein with a molecular mass of 75.3 kDa (687 residues) per monomer.[14] Its three-dimensional (3D) structure has been elucidated with bound β-mercaptoethanol [Protein Data Bank (PDB) entry 2YII] (Figure 2).[18] The enzyme is virtually identical to a PAM from *Taxus cuspidata* (*Tc*PAM, 698 residues per monomer, molecular mass of 76.5 kDa, 98% identical sequence).[19,20] Of this latter enzyme,[a] a 3D structure has been elucidated with bound *t*-CA (PDB entry 3NZ4).[21] The 3D structure of a prokaryotic PAM from *Pantoea agglomerans* (*Pa*PAM, 541 residues per monomer, molecular mass of 59.3 kDa, 21% identical sequence)[22] has been determined showing a mixture of covalently bound (*S*)-α-Phe and (*S*)-β-Phe (PDB entry

Received: February 12, 2014
Revised: April 27, 2014
Published: April 30, 2014

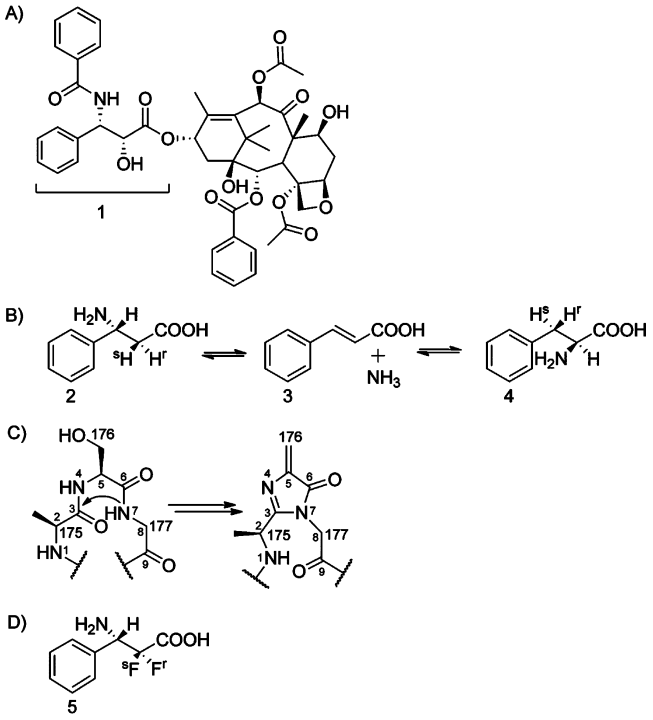

Figure 1. (A) (*R*)-*β*-Phe (**2**) is the precursor of the *N*-benzoyl-phenylisoserinoyl side chain (bracket) of Taxol synthesized by *Taxus* sp. (B) PAM-catalyzed reaction. The formation of (*R*)-*β*-Phe (**2**) and (*S*)-*α*-Phe (**4**) proceeds via *t*-CA (**3**) and requires the interchange of the amino group and the *pro*-*S* proton. (C) Chemical structure of the MIO group (right), which is formed from residues A175, S176, and G177 (left). (D) (*S*)-3-Amino-2,2-difluoro-phenylpropionic acid (**5**), an analogue of (*R*)-*β*-Phe, used for substrate analogue binding studies.

3UNV[23]). These PAMs have a sequence significantly identical (24%) to that of tyrosine aminomutase from *Streptomyces globisporus* (TAM), a protein with a molecular mass of 58.1 kDa (539 residues) per monomer.[24] The 3D structure of TAM (PDB entry 2OHY[25]) has been determined with covalently bound (*S*)-*α*-tyrosine (PDB entry 3KDZ[26]) and with covalently bound fluorinated *β*-tyrosine analogues (PDB entries 2QVE and 2RJS[27]). The PAM structures are also highly similar to the structures of *Rhodosporidium toruloides* phenylalanine ammonia lyase (PAL, 716 residues per monomer, molecular mass of 76.9 kDa, 32.8% identical sequence) with bound *t*-CA (PDB entry 1T6J),[28] *Pseudomonas putida* histidine ammonia lyase (*Pp*HAL, 510 residues per monomer, molecular mass of 53.8 kDa, 21.6% identical sequence, PDB entry 1B8F[29]), and *Rhodobacter sphaeroides* tyrosine ammonia lyase (TAL, 523 residues per monomer, molecular mass of 54.9 kDa, 21.7% identical sequence) with bound *p*-coumaric acid (PDB entry 2O7B) and caffeic acid (PDB entry 2O7D).[30]

All these proteins share a three-amino acid sequence motif (generally A-S-G but T-S-G in *Pa*PAM[23]) from which the 4-methylidene-imidazole-5-one (MIO) prosthetic group is formed by autocatalytic post-translational modifications (Figure 1C).[29] The MIO group is an electrophile, which reacts with the amino group of the substrate [*α*-phenylalanine (PAM and PAL), *α*-tyrosine (TAM and TAL), or *α*-histidine (*Pp*HAL)], and facilitates the stereoselective abstraction of one of the C*β* protons by a nearby tyrosine base[25,31−33] located in the lid loop (residues 78−97[34]) that covers the active site of the enzyme.[30] The abstraction of the proton is accompanied, sequentially or simultaneously, by the cleavage of the N−C*α* bond and leads to the formation of a product with an unsaturated C*α*−C*β* bond. Subsequently, in lyases, the unsaturated product and the amino group (as ammonia) are released into the environment.[35] In contrast, in aminomutases, the amine group (as a MIO−amine adduct) and the unsaturated product are retained in the active site and the unsaturated product is reaminated and reprotonated at the other C atom.[19,22,27] In both *Taxus*

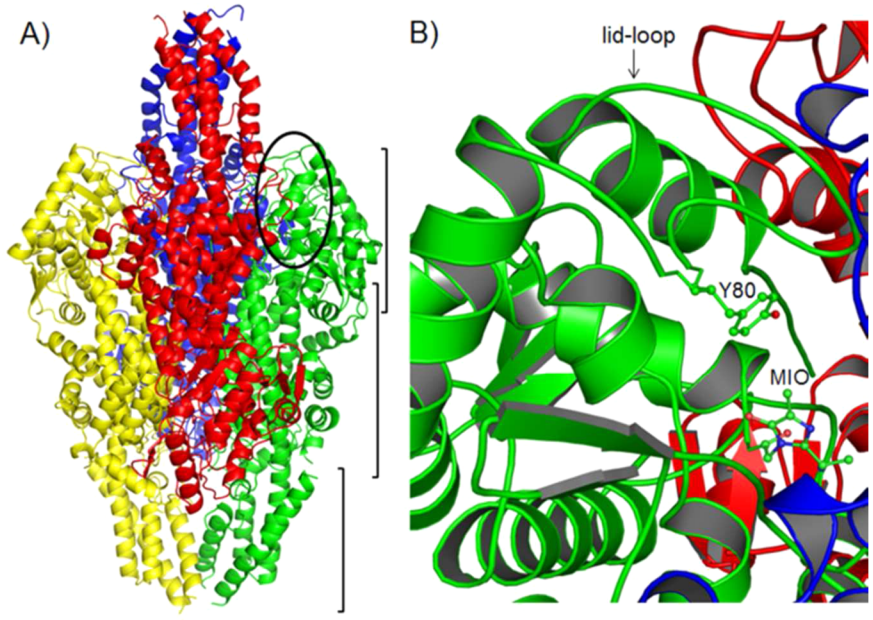

Figure 2. (A) Structure of PAM (PDB entry 2YII[18]). The four monomers are related by 222 symmetry. Monomer A is colored green, and the brackets denote the head domain, body domain, and tail domain (from top to bottom, respectively). The oval shows the approximate location of the active site of PAM, which is located in the head domain. (B) The active site of PAM is covered by the lid loop, which contains Y80 (the tyrosine base). For the sake of clarity, the *β*-mercaptoethanol molecule bound to the MIO group has been removed.

Table 1. Data collection and refinement statistics of PAM crystal structures

	WT PAM with analogue[e]	Y80A with analogue[e]	WT PAM with (*R*)-*β*-Phe	Y322A PAM[f]	N231A PAM
			Data Collection		
beamline	ID14-1	ID23-2	ID23-2	ID23-1	ID29
resolution (Å)[a]	49.09−2.14 (2.26−2.14)	48.73−1.85 (1.95−1.85)	34.06−1.90 (2.00−1.90)	48.38−2.2 (2.32−2.20)	48.91−2.1 (2.21−2.10)
space group	$P2_1$	$P2_1$	$P2_1$	$P2_1$	$P2_1$
cell dimensions					
a, *b*, *c* (Å)	99.4, 145.5, 99.6	99.8, 146.2, 100.4	99.9, 146.4, 100.5	99.5, 147.3, 99.8	99.0, 146.6, 99.3
β (deg)	99.5	99.3	99.6	99.8	100
R_{merge}[b]	0.08 (0.38)	0.07 (0.45)	0.11 (0.49)	0.05 (0.40)	0.07 (0.4)
wavelength (Å)	0.9334	0.8726	0.8726	1.710	0.9793
$I/\sigma(I)$	9.9 (3.0)	11.3 (2.3)	6.0 (2.0)	11.3 (2.6)	11.2 (2.9)
completeness (%)	99.4 (97.5)	100 (100)	99.6 (99.1)	95.4 (92.3)	99.8 (99.5)
no. of unique reflections	151434 (21709)	241051 (35117)	222303 (32224)	136388 (19209)	161887 (23559)
multiplicity	2.8 (2.7)	2.9 (2.9)	2.6 (2.6)	2.5 (2.5)	3.8 (3.7)
			Refinement		
resolution (Å)	2.20	1.90	1.90	2.2	2.10
R_{work}[c]	0.17	0.18	0.18	0.19	0.20
R_{free}[d]	0.21	0.21	0.21	0.22	0.24
root-mean-square deviation					
bond lengths (Å)	0.008	0.010	0.008	0.010	0.009
bond angles (deg)	1.25	1.30	1.27	1.37	1.28
Ramachandran (MolProbity)					
favored (%)	98.2	98.1	97.7	97.3	97.2
outliers (%)	0.00	0.00	0.00	0.04	0.00
average atomic *B* factor					
protein	25.0	19.4	25.1	41.5	46.2
ligand	30.5	20.7	28.3	not applicable	not applicable
solvent	24.7	21.3	27.1	30.6	36.3
no. of atoms per asymmetric unit	20505	20797	20824	19779	19587
Wilson *B* factor	21.3	17.8	20.4	35.3	29.6
PDB entry	4C5R	4C5S	4CQ5	4C5U	4C6G

[a]Values in parentheses are for the highest-resolution shell. [b]$R_{merge} = \sum_h\sum_i|I(h)_i - \langle I(h)\rangle|/\sum_h\sum_i\langle I(h)_i\rangle$, where I is the observed intensity and $\langle I\rangle$ is the average intensity of multiple observations of symmetry-related reflections. [c]$R_{work} = \sum_h|F_{obs} - F_{calc}|/\sum_h|F_{obs}|$, where F_{obs} and F_{calc} are the observed and calculated structure factor amplitudes, respectively. [d]R_{free} is calculated as R_{work} using 5% of all reflections randomly chosen and excluded from structure factor calculation and refinement. [e]The analogue is (*S*)-3-amino-2,2-difluoro-phenylpropanoic acid [**5** (Figure 1D)]. [f]The crystal is pseudohemihedrally twinned with a twin fraction *α* that equals 0.14. The twin operator, a 2-fold axis, is from *h*,*k*,*l* to *l*,−*k*,*h* and lies in the *a*−*c* plane of the unit cell along the diagonal between the *a* and *c* axes.

PAMs, this reaction results in the synthesis of (*R*)-*β*-Phe from (*S*)-*α*-Phe.[16,36] Thus, the PAM-catalyzed conversion can be considered to proceed via two half-reactions. In the first half-reaction, the enzyme abstracts the C*β* *pro-S* proton and the C*α* amino group from (*S*)-*α*-Phe. In the second half-reaction, the enzyme re-adds the proton to the *si* face of the C*α* atom of *t*-CA at the position formerly occupied by the amino group and re-adds the amino group to the *re* face of the C*β* atom of *t*-CA at the position formerly occupied by the *pro-S* proton (Figure 1B). In the reverse reaction, creating (*S*)-*α*-Phe from (*R*)-*β*-Phe, the enzyme interchanges the C*β* amino group with the C*α* *pro-S* proton.[19,36] The stereochemistry of the reaction requires that during the reaction the *t*-CA reaction intermediate rotates to expose the other face of the unsaturated aliphatic C−C bond to the MIO group.

Different hypotheses about how this rotation is accomplished have been formulated. Feng et al.[21] have suggested that the *t*-CA molecule that is generated during the first half-reaction rotates simultaneously around its C*γ*−C*β* and C*α*−$C^{carboxyl}$ bonds. Wang et al.[37] have suggested that the rotation occurs only around the *t*-CA molecule's C*α*−$C^{carboxyl}$ bond. Both studies assume that the *α*-carboxylate of the *t*-CA molecule remains bound to R325 in the same bidentate mode throughout the catalytic cycle. We have proposed,[18] on the basis of a comparison of PAM and TAM structures, that a rotation event occurs solely around the C*γ*−C*β* bond of the *t*-CA molecule and that the concomitant repositioning of the *α*-carboxylate group triggers the addition of an amine at the C*β* atom. Another possibility that may be considered is that the entire *t*-CA molecule rotates. However, no structural evidence has been obtained for any of these hypotheses.

Another unresolved issue of MIO-containing enzymes is the biosynthesis pathway of the MIO group. Although it is evident that a nucleophilic attack of the amide N atom of G177 on the carbonyl C atom of A175 has to occur, it is not clear how this attack is triggered. Investigations of MIO group formation in *Pp*HAL[38] implicated a glutamate residue that activates the

dx.doi.org/10.1021/bi500187a | *Biochemistry* 2014, 53, 3187−3198

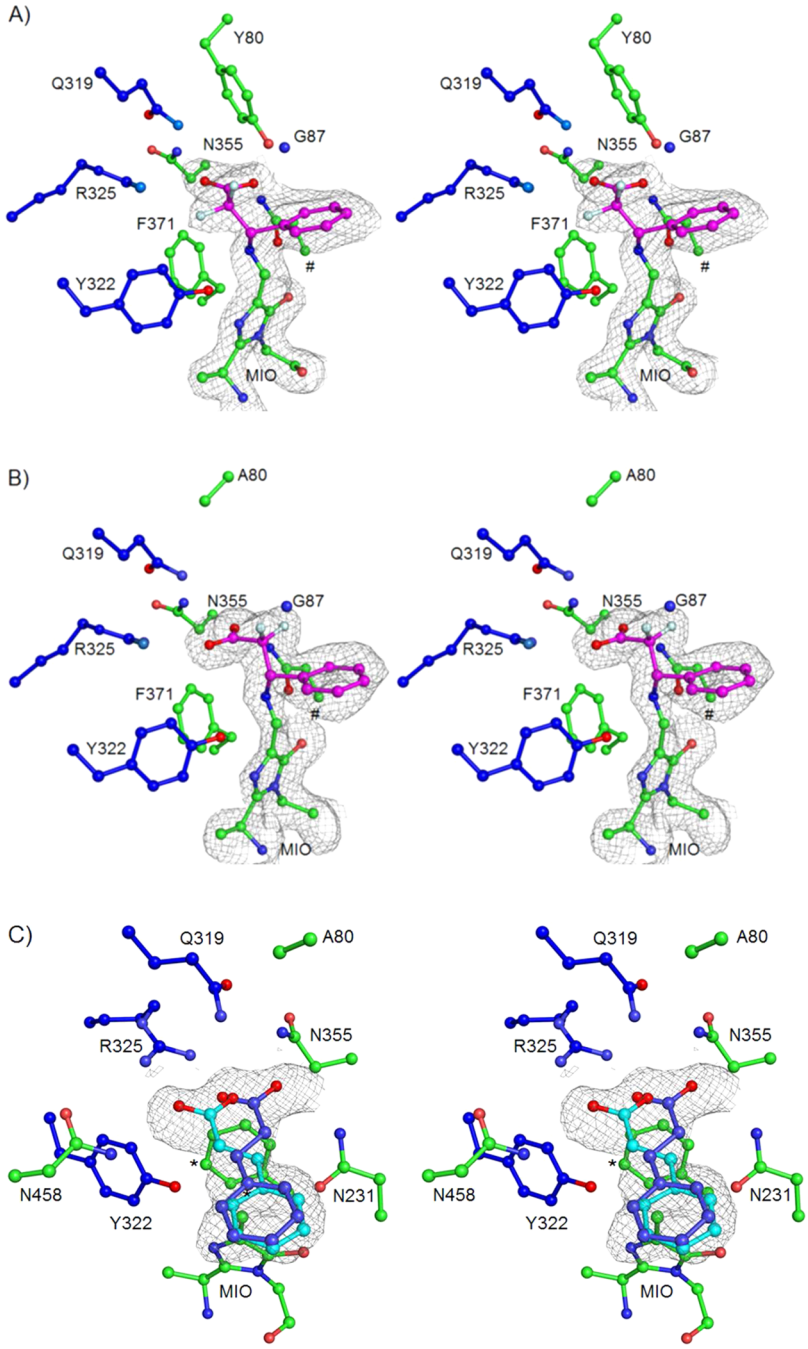

Figure 3. Stereo figures (wall-eyed) of simulated annealing composite $2mF_o - DF_c$ omit maps, contoured at 1σ. (A) Wild-type PAM with bound (*S*)-3-amino-2,2-difluoro-phenylpropionic acid (magenta). Green residues are from monomer A and blue residues from monomer B. A number sign denotes residue N231. The blue sphere represents the amide N atom of G87. (B) Y80A PAM with bound (*S*)-3-amino-2,2-difluoro-phenylpropionic acid (magenta). (C) Y80A PAM with bound *t*-CA. The *si,si* face of the cyan *t*-CA molecule (occupancy of ∼0.5) is oriented toward the MIO group, and its carboxylate group has a bidentate binding mode. The *re,re* face of the blue *t*-CA molecule (occupancy of ∼0.5) is oriented toward the MIO group, and its carboxylate group has a monodentate binding mode. The asterisk denotes residue F371. The solvent molecules (see Results) have been omitted for the sake of clarity.

amide N atom of G144. The equivalent PAM residue is a glutamine, which cannot have the same catalytic role.

Therefore, in an attempt to clarify these issues, we elucidated crystal structures of wild-type PAM and a Y80A PAM mutant in complex with a nonreactive (*R*)-*β*-Phe analogue (Figure 1D) and with bound *t*-CA. The results show that the stereochemistry of the PAM-catalyzed reaction originates from the enzyme's ability to bind *t*-CA in two different orientations. Crystal structures of the inactive Y322A and N231A PAM mutants revealed that both of them lack an intact MIO group and suggest that the N231 side chain promotes MIO group formation by increasing the nucleophilicity of the G177 N atom through acidification of the amide proton.

EXPERIMENTAL PROCEDURES

Protein Expression and Purification. Expression and purification of wild-type PAM, Y80A PAM, Y322A PAM, and N231A PAM were conducted as described by Wu et al.[18] with

dx.doi.org/10.1021/bi500187a | *Biochemistry* 2014, 53, 3187−3198

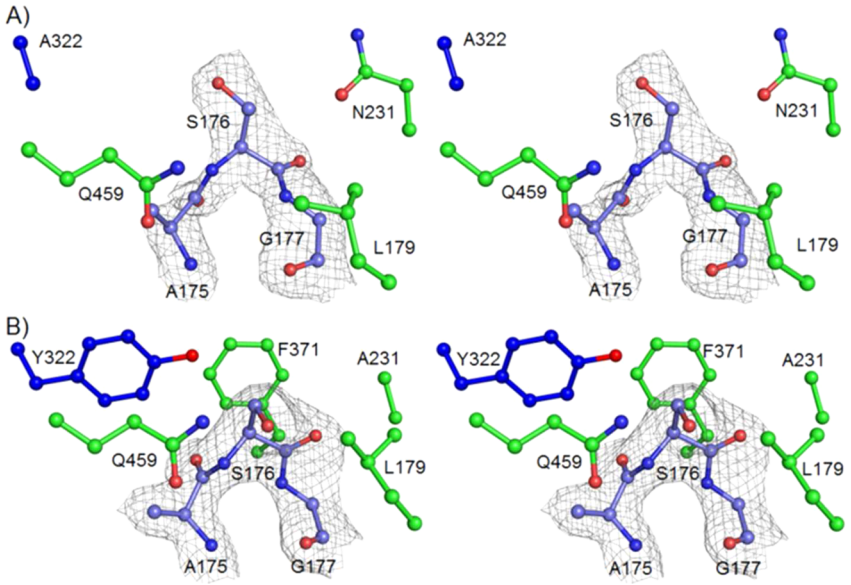

Figure 4. Stereo figures (wall-eyed) of simulated annealing composite $2mF_o - DF_c$ omit maps, contoured at 1σ. (A) Y322A mutant of PAM showing the MIO-forming loop (magenta). No density is present for F371. (B) N231A mutant of PAM showing the MIO-forming loop (magenta).

the following modifications. Wild-type PAM and Y80A PAM were purified without a reducing agent. The reducing agent [0.20 mM tris(2-carboxyethyl)phosphine (TCEP), pH adjusted to 7.0] was added to the protein sample prior to setting up crystallizations. 1,4-Dithiothreitol (DTT, 2.0 mM) was used as the reducing agent in the purification of Y322A and N231A PAM.

Protein Crystallization. The crystallization conditions and cryo-protection procedures matched those described by Wu et al.[18] For binding studies, cryoprotection solutions were supplemented with 0.20 mM TCEP (pH 7.0) and 2.0, 5.0, 10, and 20 mM ligand, and crystals were soaked for 5 min in a cryosolution before being transferred to the cryosolution with the next higher ligand concentration. (*S*)-3-Amino-2,2-difluoro-phenylpropanoic acid was synthesized using the method of Christianson et al.[39] For (*R*)-*β*-Phe binding studies, Y80A PAM was crystallized in the presence of 0.5 mM TCEP (pH 7.0) and 4.0 mM (*R*)-*β*-Phe (PepTech Corp.). After a week, crystals were soaked for 5 s in cryoprotection solutions supplemented with 0.25 mM TCEP (pH 7.0) and 2.0 mM (*R*)-*β*-Phe. Y322A and N231A PAM crystals were grown in the presence of 2.0 mM DTT and 4.0 mM *t*-CA (Acros Organics) or 2.0 mM (*S*)-*α*-Phe, respectively, which was also added to the respective cryoprotection solutions.

Collection and Processing of Diffraction Data. Diffraction data were collected at beamlines ID14-1, ID23-1, ID23-2, and ID29 of the European Synchrotron Radiation Facility (ESRF, Grenoble, France). Indexing and integration of the reflections were conducted using XDS.[40] SCALA[41] from the CCP4 software suite[42] was utilized for scaling and merging of the data. For molecular replacement, Phaser[43] was used with PAM (PDB entry 2YII[18]) as the input model. Refinement of the atomic coordinates and *B* factors was conducted with Refmac5,[44] and the model was manipulated in Coot.[45] Data collection and refinement statistics are listed in Table 1. The model quality of wild-type PAM, Y80A PAM, Y322A PAM, and N231A PAM was validated with MolProbity.[46] The PRODRG2 server[47] was used to generate the stereochemical restraints for the analogue molecule. PISA[48] was used for protein interface analysis. To generate simulated annealing composite omit maps, we utilized PHENIX.[49] Chemical structure drawings were made with ChemDraw (CambridgeSoft), and images of protein structures were made with PyMOL.[50] Atomic coordinates and structure factors have been deposited as PDB entries 4C5R, 4C5S, 4C5T, 4C5U, and 4C6G (Table 1).

Construction of PAM Mutants. Mutants of PAM were generated using the mega-primer method and the coding sequence for PAM in plasmid pBAD-His-PAM as the template.[16] The following mutagenesis primers were used: 5′-GTGGTCACGCCCGCGATATCAGCACCATCTTC-3′ for Y80A, 5′-GCCTAAACAGGACCGGGCAGCCCTGCGTAG-3′ for Y322A, and 5′-CAACTGCAGTAGCGAAGCTTGTA-CCGGCTACCAGAGCCAG-3′ for N231A (mutated codon underlined). All mutant constructs were confirmed by sequencing. All primers were supplied by Sigma-Aldrich.

RESULTS

Determination of the Structure of PAM. To provide structural insight into the ability of PAM to form (*S*)-*α*-phenylalanine [(*S*)-*α*-Phe] from (*R*)-*β*-phenylalanine [(*R*)-*β*-Phe], we elucidated crystal structures of wild-type PAM and Y80A PAM (Table S1 of the Supporting Information), both with bound (*S*)-3-amino-2,2-difluoro-phenylpropanoic acid (Figure 3A,B), an analogue of the (*R*)-*β*-Phe substrate (Figure 1D). We also elucidated a crystal structure of Y80A PAM with bound *trans*-cinnamic acid (*t*-CA) (Figure 3C), as well as structures of Y322A and N231A PAM (Figure 4A,B and Table S1 of the Supporting Information). In all cases, PAM crystallized in space group $P2_1$ with four monomers per asymmetric unit obeying 222 symmetry, similar to the wild-type protein.[18]

PAM Monomer Structure. Similar to previously published crystal structures of MIO-dependent enzymes,[21,28] the *T. chinensis* PAM monomer has an elongated shape and contains three domains, the tail domain, the body domain, and the head domain (Figure 2A). These three domains mainly consist of *α*-helices, but the head domain also contains seven short *β*-strands, which form three antiparallel *β*-sheets. The head

dx.doi.org/10.1021/bi500187a | *Biochemistry* 2014, 53, 3187−3198

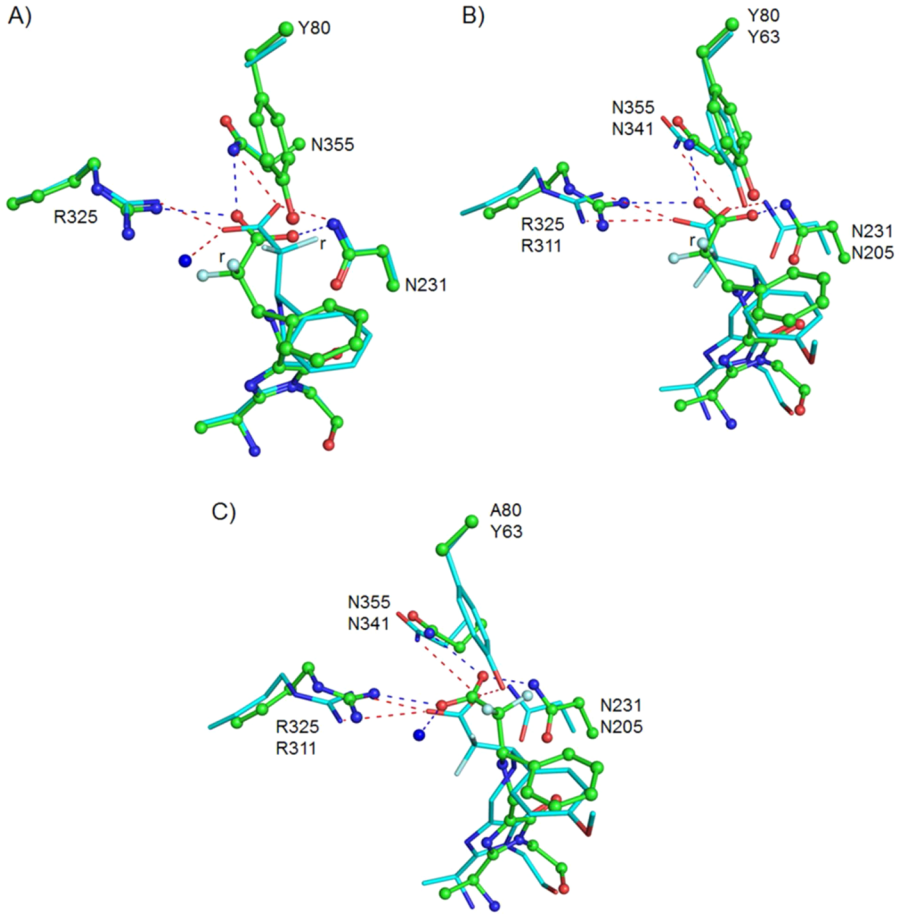

Figure 5. (A) (*R*)-*β*-Phe analogue **5** bound in the active site of wild-type PAM (green, ball and stick) superimposed on the (*R*)-*β*-Phe analogue bound in the active site of Y80A PAM (cyan sticks). The r denotes the C*α pro-R* fluorine atom. The blue sphere represents a water molecule. (B) (*R*)-*β*-Phe analogue bound in the active site of wild-type PAM (green, ball and stick) superimposed on the (*S*)-*β*-tyrosine analogue bound in the active site of TAM (cyan sticks) (PDB entry 2RJS[27]). (C) (*R*)-*β*-Phe analogue bound in the active site of Y80A PAM (green, ball and stick) superimposed on the (*S*)-*β*-tyrosine analogue bound in the active site of TAM (cyan sticks) (PDB entry 2RJS[27]).

domain contains the MIO group and the lid loop (residues 78−97), which covers the active site (Figure 2B).

PAM Tetramer Structure. As previously found, four PAM monomers (A−D) assemble into a dimer of dimers (Figure 2A).[18] The most extensive contacts are between monomers A and B, and between monomers C and D, with buried surface areas of ∼7600 Å^2 per pair. The A−C pair and the B−D pair also have extensive contacts (∼7400 Å^2 of buried surface area per pair). The head domain of monomer A interacts with the body domains of monomers B and C, while its body domain contacts the head domains of monomers B and C. The contacts between the A−D pair and the B−C pair are much less extensive (∼2300 Å^2 of buried surface area per pair), and only the tail domains take part in this interaction. The four monomers bury a total area of ∼34500 Å^2, while the total surface area of the PAM tetramer is ∼73000 Å^2. A large fraction of the PAM monomer surface is thus involved in tetramerization.

MIO Prosthetic Group. The MIO group is located in the head domain; it is post-translationally formed from the three-amino acid A175-S176-G177 sequence motif (Figure 1C). Besides the covalent main chain peptide bonds to S174 and N178, the MIO group is held in position by hydrogen bonds between the MIO O2 atom and the N*δ* atom of N231 and between the MIO N2 atom and the hydroxyl group of Y322 (monomer B when the MIO group is from monomer A). The MIO further forms aromatic interactions with F371 and L179, residues that are located at the *re* and *si* faces of the C*β*2 atom of the MIO group, respectively (Figure 6).

Structures of Wild-Type and Y80A PAM with a Bound (*R*)-*β*-Phe Analogue. To analyze how (*R*)-*β*-Phe binds in the active site of wild-type PAM, we determined a crystal structure of PAM with bound (*S*)-3-amino-2,2-difluoro-phenylpropanoic acid, an analogue of (*R*)-*β*-Phe, at 2.2 Å resolution (Figures 3A and 5A). The following description is for monomer A, but in the other PAM monomers, the situation is equivalent. The analogue is covalently bound via its *β*-amino group to the C*β*2 atom of the MIO group, and the aromatic ring is bound in a hydrophobic pocket (not shown) lined with residues from monomers A (F86, L104, V230, C107, L108, L179, L227, E455, N458, and Q459) and C (the apolar part of the side chain of K427). One of the analogue's *α*-carboxylate O atoms is within hydrogen bonding distance of the N*δ* atom of N355 (monomer A) and the N*η*2 atom of R325 (monomer B) (Figure 3A). The other *α*-carboxylate O atom (O1) is within hydrogen bonding distance of the N*δ* atom of N231. The C*α pro-S* fluorine atom of the analogue, which represents the *pro-S* proton of (*R*)-*β*-Phe, is positioned between the side chains of Y322 and R325 (monomer B), near the Y322 hydroxyl O atom and the N*η*1 and N*η*2 atoms of R325. The C*α pro-R* fluorine

dx.doi.org/10.1021/bi500187a | *Biochemistry* 2014, 53, 3187−3198

atom of the analogue is close (2.5 Å) to the hydroxyl O atom of Y80 and near (3.1 Å) the amide N atom of G87, a residue that is part of the lid loop. In this conformation, the analogue has an Nβ−Cβ−Cα−F$^{pro\text{-}R}$ dihedral angle of −165°, which is near the angle of 180° expected for the *trans* elimination of the β-amino group and the Cα *pro-R* proton. However, the conversion of (*R*)-β-Phe into (*S*)-α-Phe requires the abstraction of the Cα *pro-S* proton,[19,36] which is not feasible if the substrate adopts the binding mode of the analogue, because the Cα *pro-S* proton would not be properly oriented for a *trans* (or *cis*) elimination reaction and would not be near Y80 or another residue that could function as a base. Thus, in this structure, the conformation of the analogue does not correspond to the stereochemistry of the PAM-catalyzed reaction.

In addition, a 1.9 Å resolution crystal structure of the inactive Y80A PAM mutant was elucidated with the same (*R*)-β-Phe analogue bound. Similar to that of the wild-type complex, the structure revealed a covalent bond between the β-amino group of the analogue and the Cβ2 atom of the MIO group, with the aromatic ring of the analogue binding in the same position as in wild-type PAM. However, the α-carboxylate group of the analogue adopts a different conformation, resulting in different positions of the Cα *pro-R* and *pro-S* fluorine atoms (Figures 3B and 5A). The α-carboxylate's O1 atom has hydrogen bonding interactions with the Nδ atoms of N231 and N355, while the other O atom has hydrogen bonds with the Nη2 atom of R325 (monomer B) and a solvent molecule. Two solvent molecules are present at the location of the aromatic ring of Y80 in wild-type PAM. They are within hydrogen bonding distance of the fluorine atoms of the analogue. The Nβ−Cβ−Cα−F$^{pro\text{-}R}$ dihedral angle is −82° instead of −165° as observed in the complex with wild-type PAM, showing that the side chain of residue 80 has a dramatic influence on the binding mode of the analogue. The Nβ−Cβ−Cα−F$^{pro\text{-}S}$ dihedral angle of the analogue is 163°, which is compatible with a geometry that allows the *trans* elimination of the Cα *pro-S* proton and the β-amino group.

Structure of Y80A PAM Bound to *trans*-Cinnamic Acid. We cocrystallized (inactive) Y80A PAM with (*R*)-β-Phe to try to analyze true substrate binding interactions. However, a 1.9 Å resolution simulated annealing composite $2mF_o - DF_c$ omit electron density map (Figure 3C) revealed a non-covalently bound *t*-CA molecule in the active site, suggesting that (*R*)-β-Phe had been deaminated, in spite of Y80A PAM being inactive. The *t*-CA molecule was bound in two orientations (each with an occupancy of ∼0.5), with either the *si,si* face or the *re,re* face oriented toward the MIO group. In both orientations, the *t*-CA aromatic ring binds in the hydrophobic binding pocket in a position similar to that of the aromatic ring of the (*R*)-β-Phe analogue in wild-type and Y80A PAM, but the *t*-CA α-carboxylate group has different interactions. If the *si,si* face of the *t*-CA molecule is directed toward the MIO group, the α-carboxylate group interacts via both O atoms in a bidentate mode with the side chain Nη atoms of R325, with additional hydrogen bonding interactions to the Nδ atom of N458 and, via a solvent molecule, to the Nδ atoms of N231 and N355 (Figure 3C, cyan molecule). When the *re,re* face is oriented toward the MIO group, the α-carboxylate group interacts via one O atom (monodentate mode) with the R325 side chain, and the other carboxylate O atom is hydrogen bonded to the Nδ atoms of N231 and N355 (Figure 3C, blue molecule). This latter binding mode resembles the binding of the α-carboxylate group of the (*R*)-β-Phe analogue in Y80A PAM.

Structure of Y322A PAM. To obtain details about the roles of other essential residues in the active site of PAM, we determined the crystal structures of Y322A and N231A PAM (Table S1 of the Supporting Information), both of which are inactive. The 2.2 Å resolution structure of Y322A PAM revealed that all monomers are MIO-less (Figure 4A). In monomers A, C, and D, residues A175-S176-G177 are present as a peptide loop; in monomer B, residues 175−177 have no defined electron density. In monomers A, C, and D, the A175 carbonyl C atom is 3.3 Å from the amide N atom of G177. S176, in the center of the MIO-forming loop, is located in a position that in wild-type PAM is occupied by the aromatic ring of F371 (Figure 6A); in Y322A PAM, F371 and its flanking residues 368−372 are not defined in the electron density maps. Thus, our results show that Y322 is essential for MIO group formation and that Y322A PAM is inactive because of the absence of a functional MIO group.

Structure of N231A PAM. The 2.1 Å resolution crystal structure of N231A PAM (Figure 4B) revealed that all four of its monomers are MIO-less and contain an unreacted MIO-forming loop (residues A175-S176-G177), which takes up the same space as the MIO group in wild-type PAM (Figure 6B). The absence of a functional MIO group explains the lack of catalytic activity of N231A PAM. Interestingly, in the four monomers, the distance between the amide N atom of G177 and the carbonyl C atom of A175 is 2.8 Å, which would be compatible with a nucleophilic attack of the G17 N atom on the A175 carbonyl C atom. Nevertheless, this reaction has not occurred, demonstrating that the N231 side chain is essential for MIO group formation.

The structure of N231A PAM also shows that the mutation has resulted in significant conformational flexibility and/or disorder of residues 78−98. In monomer B, residues 78−86 have a conformation similar to that of wild-type PAM, but in the other monomers, they have moved away from the active site (Figure 7). The residues in the second part of the loop (residues 87−98) are disordered and have no interpretable electron density. This conformational flexibility or disorder suggests that the N231 side chain is important for stabilizing the conformation of the lid loop (residues 78−98[34]).

DISCUSSION

To explain how the *Taxus* PAMs catalyze the interchange of an amino group and a proton at neighboring C atoms, we have elucidated crystal structures of wild-type PAM with a bound (*R*)-β-phenylalanine analogue, Y80A PAM with the same analogue, and Y80A PAM with bound *t*-CA (Figure 3A−C). In addition, we have elucidated structures of Y322A and N231A PAM, which are both inactive and MIO-less (Figure 4A,B). In all cases, the structures are highly similar to the structure of wild-type PAM, except for residues 78−98 in the N231A mutant, which show conformational flexibility and/or disorder (see Results).

Y322 and N231 Are Essential for MIO Group Formation. Previous screening experiments showed that Y322 and N231 are essential for PAM activity.[18] Indeed, Y322A and N231A PAM are both inactive (Table S1 of the Supporting Information). Their 3D structures revealed that they do not have an intact MIO group (Figures 4 and 6), explaining their lack of activity, and indicating that Y322 and

dx.doi.org/10.1021/bi500187a | *Biochemistry* 2014, 53, 3187−3198

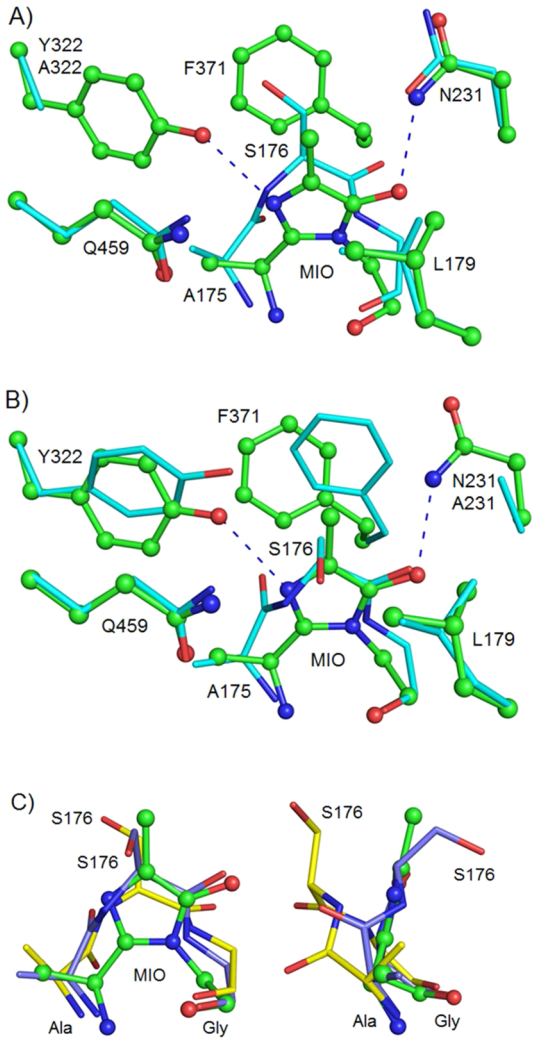

Figure 6. (A) Structure of wild-type PAM (green, ball and stick) superimposed on the structure of Y322A PAM (cyan sticks). Electron density for F371 is absent in Y322A PAM. In wild-type PAM, the Nδ atom of the N231 side chain is within hydrogen bonding distance of the O2 atom of the MIO group. In Y322A PAM, the Nδ atom of the N231 side chain is within hydrogen bonding distance of the carbonyl O atom of N355 (also see Figure 4A). (B) Structure of wild-type PAM (green, ball and stick, PDB entry 2YII[18]) superimposed on the structure of N231A PAM (cyan sticks). (C) Structure of wild-type PAM (green, ball and stick) superimposed on the structures of Y322A PAM (yellow sticks) and N231A PAM (magenta sticks). The right panel has been rotated 90° counterclockwise, along the *c* axis, with respect to the left panel.

N231 are essential for the formation of the MIO group, either directly or indirectly.

In N231A PAM, the MIO-forming loop (residues 175−177) has a conformation that corresponds to the conformation of the fully formed MIO group (Figure 6B,C). The G177 N atom is near the carbonyl C atom of A175 (at 2.8 Å) and in a position suitable for nucleophilic attack to initiate the condensation reaction toward the MIO group. Because this condensation reaction has not occurred, this suggests that the G177 N atom in N231A PAM is not sufficiently activated for such a nucleophilic attack. Baedeker and Schulz[38] have suggested that in *P. putida* HAL the equivalent N atom (G144) is activated by E414 via a water molecule. A water molecule is also present in N231A PAM, between the G177 N atom and the

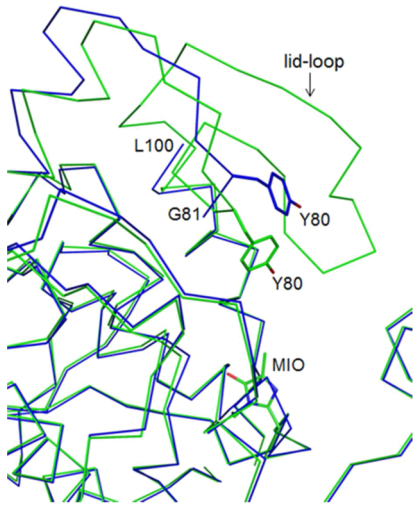

Figure 7. Monomer A of wild-type PAM (the green Cα trace) superimposed on monomer A of N231A PAM (the blue Cα trace).

side chain of Q459, the residue equivalent to E414. The Q459 side chain is, however, not in an environment that could facilitate water molecule deprotonation (Figure 6). Other residues near the MIO-forming loop, such as F371, L179, and Y322 (Figure 6), are also unlikely to participate in an activation mechanism, because they are either chemically inert or too far from the G177 N atom. The only polar residue that is near the G177 N atom is residue N231 (Figure 6A). In wild-type PAM, the N231 side chain Nδ atom is within hydrogen bonding distance to the MIO O2 atom. We therefore envisage that during MIO group formation the interaction between the N231 Nδ atom and the carbonyl O atom of S176 may increase the nucleophilicity of the G177 N atom, which may promote MIO group formation. A similar interaction between an Arg side chain and a peptide carbonyl oxygen atom has been proposed to enhance the nucleophilicity of the peptide nitrogen atom involved in the biosynthesis of the chromophore of green fluorescent protein.[51,52] Quantum chemical calculations may further validate this proposal for PAM. Just as N231A PAM, the Y322A PAM mutant is inactive because the MIO group has not been formed. The MIO-forming loop (residues 175−177) has a conformation that is not very favorable for the nucleophilic attack of the G177 N atom on the carbonyl C atom of A175. The majority of the atoms of the MIO-forming loop, in contrast to the atoms of the MIO-forming loop in N231A PAM, do not take up the same space as the MIO group in wild-type PAM (Figure 6A,C). In addition, the carbonyl O atom of S176, in the center of the MIO-forming loop, is too far from the Nδ atom of the N231 side chain for a hydrogen bonding interaction, precluding activation of the G177 N atom for nucleophilic attack (Figure 6A). A possible function of the Y322 side chain could thus be to position the A175 carbonyl C atom in a location where it can be attacked by the G177 N atom of the MIO-forming loop.

Unproductive Binding of the Substrate Analogue. The (*R*)-β-Phe substrate analogue (*S*)-3-amino-2,2-difluoro-phenyl-propanoic acid binds covalently to the MIO group via its β-amino group (Figure 5A), which is similar to what has been observed for fluorine-substituted analogues of β-tyrosine.[27] In both wild-type and Y80A PAM, the aromatic ring is bound in a hydrophobic binding pocket, but the carboxylate group takes

dx.doi.org/10.1021/bi500187a | *Biochemistry* 2014, 53, 3187−3198

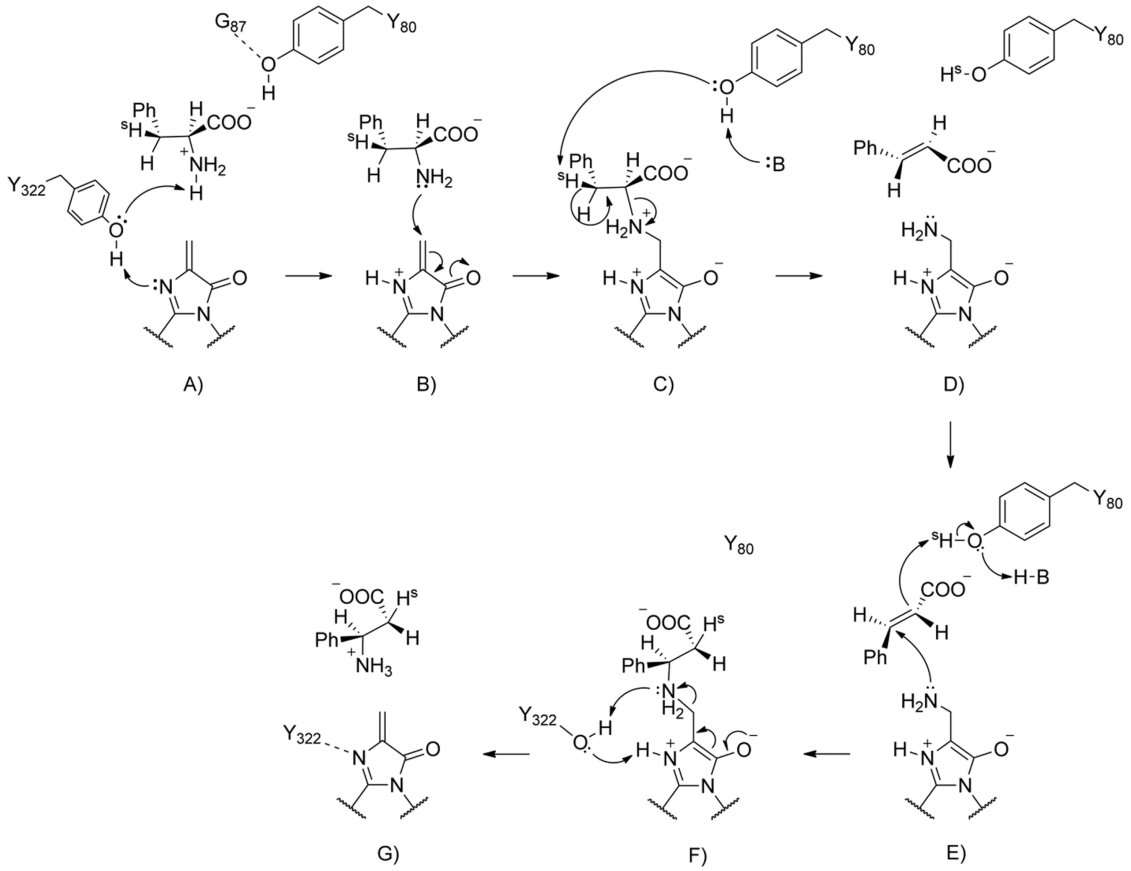

Figure 8. Proposed reaction mechanism of PAM. The scheme shows the formation of (*R*)-*β*-Phe from (*S*)-*α*-Phe via *t*-CA. (A) The reaction starts with (*S*)-*α*-Phe entering the active site. The amino group is activated by residue Y322. (B) Nucleophilic attack of the amine group onto the methylidene of the MIO group. (C) The C*β* *pro-S* proton is abstracted by Y80 (B is a base that currently still has not been identified). The amine group is abstracted by the MIO group. (D) Formation of the MIO−amine adduct and formation of *t*-CA (the *si,si* face of the *t*-CA molecule is oriented toward the MIO group). The *t*-CA molecule undergoes a rotation event, after which the *t*-CA molecule displays the *re,re* face to the aminated MIO group. (E) The *pro-S* proton is re-added to the C*α* atom of *t*-CA, while the amine group is re-added to the C*β* atom of *t*-CA. (F and G) Formation of (*R*)-*β*-Phe. The formation of (*S*)-*α*-Phe from (*R*)-*β*-Phe proceeds in the reverse order. The release of *t*-CA occurs at step D (see the introductory section). Proton shuttling and MIO aromatization adapted from ref 53.

different positions, as do, by consequence, the C*α* fluorine atoms (Figures 3B and 5A).

As argued in the Results, the binding mode of the analogue observed in wild-type PAM is not compatible with productive binding of a true substrate. The unproductive binding mode is the result of the two electronegative fluorine atoms maximizing their interactions with the enzyme. The *pro-S* fluorine and one of the *α*-carboxylate O atoms interact with the R325 side chain, while the *pro-R* fluorine has a hydrogen bonding interaction with the Y80 hydroxyl group. Removing this latter interaction (as in the Y80A mutant) yields a different rotamer, with only the *pro-S* fluorine interacting with the protein (with the G87 peptide N atom, which is near the position of the Y80 OH group in the wild-type enzyme). This latter binding mode is compatible with productive binding of a substrate, allowing *trans* elimination of the C*α* *pro-S* proton and the *β*-amino group. We conclude that the unproductive binding mode of the analogue is caused by the partial negative charge on the fluorine atoms. The electronegative fluorine atoms promote different interactions with the protein compared to those of a true substrate, in which the C*α* H atoms are not electronegative.

The *trans*-Cinnamic Acid Binding Modes Explain the Substrate Specificity and Stereospecificity of PAM. A cocrystallization experiment with (inactive) Y80A PAM with (*R*)-*β*-Phe revealed the binding mode of *t*-CA in the active site, instead of (*R*)-*β*-Phe (Figure 3C). This suggests that the substrate had reacted, even though the catalytic tyrosine was absent. Conceivably, water molecules that fill the space vacated by the phenyl ring upon mutation were, together with the MIO group, instrumental in proton transfer and cleavage of the MIO adduct. Alternatively, the *t*-CA molecule bound in the active site of Y80A PAM might originate from a *t*-CA contamination in the (*R*)-*β*-Phe solution used to prepare the cocrystallization experiment.

Nevertheless, the binding modes of *t*-CA provide a rationale for the enzyme's substrate specificity, which has been extensively investigated.[15−17] PAM deaminates phenylalanine and aminates *t*-CA and various apolar *ortho-*, *meta-*, and *para*-substituted *t*-CA derivatives. From the structure, it is clear that the hydrophobic binding pocket of PAM is narrower near the *meta* and *ortho* positions of the *t*-CA aromatic ring, which correlates well with the observation that PAM accepts only rather small *ortho-* and *meta*-fluoro-, chloro-, bromo-, and methyl-substituted cinnamic acid derivatives. The presence of several aromatic residues that line the hydrophobic binding pocket of PAM explains the enzyme's affinity for derivatives of *t*-CA with apolar substituents.

dx.doi.org/10.1021/bi500187a | *Biochemistry* 2014, 53, 3187−3198

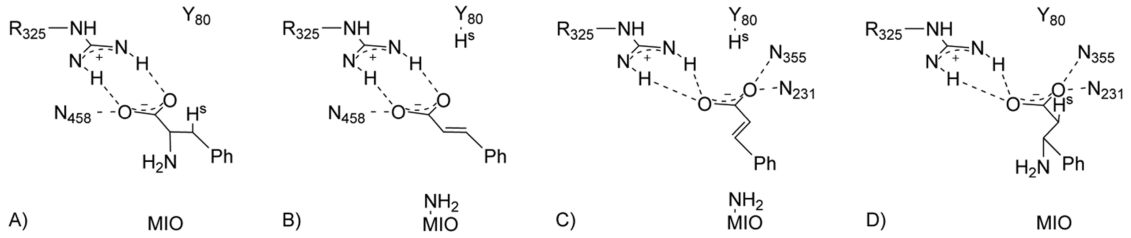

Figure 9. Carboxylate binding modes observed in aminomutases and their relevance for the (*S*)-*α*-Phe → (*R*)-*β*-Phe isomerization reaction. (A) Proposed binding mode of (*S*)-*α*-Phe (see Discussion). (B) Carboxylate binding mode observed for *t*-CA in Y80A PAM (Figure 3C, cyan molecule). This carboxylate binding mode is proposed to reflect the carboxylate binding mode of *t*-CA after *α*-elimination. The *si,si* face of the *t*-CA molecule is directed toward the MIO group, and the *re,re* face is directed toward Y80. (C) Carboxylate binding mode observed for *t*-CA in Y80A PAM (Figure 3C, blue molecule). This binding mode is proposed to reflect the carboxylate binding mode of *t*-CA after *β*-elimination. The *re,re* face of the *t*-CA molecule is directed toward the MIO group. (D) Carboxylate binding mode observed for the difluoro inhibitor **5** (Figures 1D and 3B) in Y80A PAM. This binding mode is proposed to resemble the binding mode of (*R*)-*β*-Phe in wild-type PAM.

In addition, the two *t*-CA binding modes, with either the *re,re* face or the *si,si* face oriented toward the MIO group, explain the stereochemistry of the PAM-catalyzed isomerization reaction. For the aminomutase reaction, the *t*-CA molecule must undergo a rotation, because upon deamination of (*S*)-*α*-Phe the *si,si* face of the *t*-CA molecule is oriented to the MIO−amine adduct, whereas subsequent formation of (*R*)-*β*-Phe requires that the *re,re* face of *t*-CA be oriented toward the MIO−amine adduct (Figure 8). Our structures show for the first time that the PAM active site can indeed accommodate the reaction intermediate (*t*-CA) in two different orientations, exposing either the *re,re* face or the *si,si* face to the MIO group. The electron density maps did not reveal other conformations that would support a specific rotation mechanism such as that proposed by Feng et al.,[21] Wu et al.,[18] or Wang et al.[37] A rotation of the entire *t*-CA molecule may be energetically favorable because it does not break the *π* conjugation within the *t*-CA molecule, which is especially problematic in the case of a double internal rotation around both the C*γ*−C*β* and C*α*−$C^{carboxyl}$ bonds, as proposed by Feng et al.[21,37] On the other hand, rotation of the entire *t*-CA molecule would probably require flexibility of the residues lining active site. Nevertheless, breathing motions of the protein or movements of the lid loop (residues 78−98[34]), which covers the active site, may create sufficient space for such a rotation, without letting the *t*-CA reaction intermediate escape into the solvent.

Interestingly, the different *t*-CA orientations show different *α*-carboxylate interactions. These differences in the carboxylate binding modes have been proposed to play a role in PAM regioselectivity, because interactions of carboxylate O atoms influence the delocalization of negative charge to the *α*-carboxylate group or to the phenyl ring during the addition of *t*-CA to the MIO−NH_2 adduct.[18] An increased level of delocalization of negative charge to the *α*-carboxylate group of *t*-CA was proposed to stimulate *β*-addition,[18] in agreement with the observation that electron-donating groups on the phenyl ring promote *β*-addition whereas electron-withdrawing substituents cause preferential *α*-addition of the amine to *t*-CA.[16,17]

The two carboxylate binding modes observed for *t*-CA in the crystal structures, in combination with the stereochemical,[19,20] chemical,[16,17] and biochemical[18] evidence, can now rationalize the enzyme's reaction specificity. If the *si,si* face of *t*-CA is directed toward the MIO group, the carboxylate group interacts via both O atoms (bidentate binding mode) with the side chain N*η* atoms of R325, with an additional hydrogen bonding interaction to the N*δ*2 atom of N458 (Figures 3C and 9B). This binding mode does not give optimal stabilization of the negative charge over the *t*-CA carboxylate and promotes *α*-reactivity.[18] When the *re,re* face is oriented toward the MIO group, the carboxylate group has hydrogen bonding interactions via one O atom with both R325 side chain N*η* atoms (monodentate binding mode), and the other carboxylate O atom is hydrogen bonded to the N*δ*2 atoms of N355 and N231 (Figures 3C and 9C). With four hydrogen bonds instead of three, this binding mode gives better stabilization of the delocalized negative charge and would thereby enhance *β*-reactivity according to a Michael-type 1,4-addition.

Our results suggest a possible pathway for the isomerization reaction that starts with binding of (*S*)-*α*-Phe in the active site (Figure 9A). After elimination of the amino group, *t*-CA is formed, and the carboxylate group interacts with R325 in a bidentate binding mode (Figure 9B). This binding mode was proposed by Wu et al.[18] to promote *α*-reactivity. For the next step of the reaction (addition of the amino group to the C*β* atom of *t*-CA), the *t*-CA molecule undergoes a rotation event, with a concomitant change of its carboxylate binding mode, from bidentate to monodentate (Figure 9C). The molecule is then aminated to form (*R*)-*β*-Phe (Figure 9D). The different carboxylate binding sites in the PAM active site pocket thus facilitate the required rotation of the *t*-CA molecule in the active site pocket of the enzyme, after which the *t*-CA molecule can become reaminated at the opposite face and at the flanking C atom. This sequence of events is in full agreement with the observed reaction specificity of PAM.

We propose that the two distinct carboxylate binding modes have evolved in PAM to allow the enzyme to reversibly interconvert (*S*)-*α*-Phe and (*R*)-*β*-Phe.

■ ASSOCIATED CONTENT

Supporting Information

Specific activities of wild-type PAM and its mutants (Table S1). This material is available free of charge via the Internet at http://pubs.acs.org.

■ AUTHOR INFORMATION

Corresponding Author

*Telephone: +31-50-3634378. Fax: +31-50-3634800. E-mail: b.w.dijkstra@rug.nl.

Funding

This project was financially supported by The Netherlands Ministry of Economic Affairs and the B-Basic partner organizations through B-Basic, a public-private NWO-ACTS

program (ACTS, Advanced Chemical Technologies for Sustainability), and by the European Union's Seventh Framework Program FP7/2007-2013 under Grant 266025 (BioNexGen).

Notes

The authors declare no competing financial interest.

■ ACKNOWLEDGMENTS

We acknowledge the European Synchrotron Radiation Facility (ESRF) for provision of synchrotron radiation facilities. We thank the beamline staff of ID14-1, ID23-1, ID23-2, and ID29 for their assistance. We further thank Dr. A. C. Terwisscha van Scheltinga for help with twinning analysis.

■ ABBREVIATIONS

(*R*)-*β*-Phe, (*R*)-*β*-phenylalanine; (*S*)-*α*-Phe, (*S*)-*α*-phenylalanine; (*S*)-*β*-Phe, (*S*)-*β*-phenylalanine; *t*-CA, *trans*-cinnamic acid; MIO, 4-methylidene-imidazole-5-one; PAM, *T. chinensis* phenylalanine-2,3-aminomutase; *Tc*PAM, *T. cuspidata* phenylalanine-2,3-aminomutase; *Pa*PAM, *P. agglomerans* phenylalanine-2,3-aminomutase; TAM, *S. globisporus* tyrosine-2,3-aminomutase; PAL, *R. toruloides* phenylalanine ammonia lyase; *Pp*HAL, *Ps. putida* histidine ammonia lyase; TAL, *Rh. sphaeroides* tyrosine ammonia lyase.

■ ADDITIONAL NOTE

[a]*T. cuspidata* PAM and *T. chinensis* PAM have the same GenBank accession number (AY582743).

■ REFERENCES

(1) Juaristi, E., and Soloshonok, V. A. (2005) *Enantioselective synthesis of β-amino acids*, 2nd ed., Wiley & Sons, Hoboken, NJ.

(2) Weiner, B., Szymanski, W., Janssen, D. B., Minnaard, A. J., and Feringa, B. L. (2010) Recent advances in the catalytic asymmetric synthesis of *β*-amino acids. *Chem. Soc. Rev. 39*, 1656−1691.

(3) Wani, M. C., Taylor, H. L., Wall, M. E., Coggon, P., and McPhail, A. T. (1971) Plant antitumor agents. VI. The isolation and structure of taxol, a novel antileukemic and antitumor agent from *Taxus brevifolia*. *J. Am. Chem. Soc. 93*, 2325−2327.

(4) Rowinsky, E. K. (1997) The development and clinical utility of the taxane class of antimicrotubule chemotherapy agents. *Annu. Rev. Med. 48*, 353−374.

(5) Nicolaou, K. C., Dai, W., and Guy, R. K. (1994) Chemistry and biology of taxol. *Angew. Chem., Int. Ed. 33*, 15−44.

(6) Holton, R. A., Somoza, C., Kim, H. B., Liang, F., Biediger, R. J., Boatman, P. D., Shindo, M., Smith, C. C., and Kim, S. (1994) First total synthesis of taxol. 1. Functionalization of the B ring. *J. Am. Chem. Soc. 116*, 1597−1598.

(7) Holton, R. A., Kim, H. B., Somoza, C., Liang, F., Biediger, R. J., Boatman, P. D., Shindo, M., Smith, C. C., and Kim, S. (1994) First total synthesis of taxol. 2. Completion of the C and D rings. *J. Am. Chem. Soc. 116*, 1599−1600.

(8) Nicolaou, K. C., Yang, Z., Liu, J. J., Ueno, H., Nantermet, P. G., Guy, R. K., Claiborne, C. F., Renaud, J., Couladouros, E. A., and Paulvannan, K. (1994) Total synthesis of taxol. *Nature 367*, 630−634.

(9) Suffness, M. (1995) *Taxol: Science and applications*, CRC Press, Boca Raton, FL.

(10) Guerra-Bubb, J., Croteau, R., and Williams, R. M. (2012) The early stages of taxol biosynthesis: An interim report on the synthesis and identification of early pathway metabolites. *Nat. Prod. Rep. 29*, 683−696.

(11) Lataste, H., Senilh, V., Wright, M., Guenard, D., and Potier, P. (1984) Relationships between the structures of taxol and baccatine III derivatives and their *in vitro* action on the disassembly of mammalian brain and *Physarum* amoebal microtubules. *Proc. Natl. Acad. Sci. U.S.A. 81*, 4090−4094.

(12) Fleming, P. E., Mocek, U., and Floss, H. G. (1993) Biosynthesis of taxoids. Mode of formation of the taxol side chain. *J. Am. Chem. Soc. 115*, 805−807.

(13) Walker, K. D., and Floss, H. G. (1998) Detection of a phenylalanine aminomutase in cell-free extracts of *Taxus brevifolia* and preliminary characterization of its reaction. *J. Am. Chem. Soc. 120*, 5333−5334.

(14) Steele, C. L., Chen, Y., Dougherty, B. A., Li, W., Hofstead, S., Lam, K. S., Xing, Z., and Chiang, S. J. (2005) Purification, cloning, and functional expression of phenylalanine aminomutase: The first committed step in taxol side-chain biosynthesis. *Arch. Biochem. Biophys. 438*, 1−10.

(15) Klettke, K. L., Sanyal, S., Mutatu, W., and Walker, K. D. (2007) *β*-Styryl- and *β*-aryl-*β*-alanine products of phenylalanine aminomutase catalysis. *J. Am. Chem. Soc. 129*, 6988−6989.

(16) Wu, B., Szymanski, W., Wietzes, P., de Wildeman, S., Poelarends, G. J., Feringa, B. L., and Janssen, D. B. (2009) Enzymatic synthesis of enantiopure *α*- and *β*-amino acids by phenylalanine aminomutase-catalysed amination of cinnamic acid derivatives. *ChemBioChem 10*, 338−344.

(17) Szymanski, W., Wu, B., Weiner, B., de Wildeman, S., Feringa, B. L., and Janssen, D. B. (2009) Phenylalanine aminomutase-catalyzed addition of ammonia to substituted cinnamic acids: A route to enantiopure *α*- and *β*-amino acids. *J. Org. Chem. 74*, 9152−9157.

(18) Wu, B., Szymanski, W., Wybenga, G. G., Heberling, M. M., Bartsch, S., de Wildeman, S., Poelarends, G. J., Feringa, B. L., Dijkstra, B. W., and Janssen, D. B. (2012) Mechanism-inspired engineering of phenylalanine aminomutase for enhanced *β*-regioselective asymmetric amination of cinnamates. *Angew. Chem., Int. Ed. 51*, 482−486.

(19) Walker, K. D., Klettke, K., Akiyama, T., and Croteau, R. (2004) Cloning, heterologous expression, and characterization of a phenylalanine aminomutase involved in taxol biosynthesis. *J. Biol. Chem. 279*, 53947−53954.

(20) Jennewein, S., Wildung, M. R., Chau, M., Walker, K., and Croteau, R. (2004) Random sequencing of an induced taxus cell cDNA library for identification of clones involved in taxol biosynthesis. *Proc. Natl. Acad. Sci. U.S.A. 101*, 9149−9154.

(21) Feng, L., Wanninayake, U., Strom, S., Geiger, J., and Walker, K. D. (2011) Mechanistic, mutational, and structural evaluation of a *Taxus* phenylalanine aminomutase. *Biochemistry 50*, 2919−2930.

(22) Ratnayake, N. D., Wanninayake, U., Geiger, J. H., and Walker, K. D. (2011) Stereochemistry and mechanism of a microbial phenylalanine aminomutase. *J. Am. Chem. Soc. 133*, 8531−8533.

(23) Strom, S., Wanninayake, U., Ratnayake, N. D., Walker, K. D., and Geiger, J. H. (2012) Insights into the mechanistic pathway of the *Pantoea agglomerans* phenylalanine aminomutase. *Angew. Chem., Int. Ed. 51*, 2898−2902.

(24) Christenson, S. D., Liu, W., Toney, M. D., and Shen, B. (2003) A novel 4-methylideneimidazole-5-one-containing tyrosine aminomutase in enediyne antitumor antibiotic C-1027 biosynthesis. *J. Am. Chem. Soc. 125*, 6062−6063.

(25) Christianson, C. V., Montavon, T. J., Van Lanen, S. G., Shen, B., and Bruner, S. D. (2007) The structure of L-tyrosine 2,3-aminomutase from the C-1027 enediyne antitumor antibiotic biosynthetic pathway. *Biochemistry 46*, 7205−7214.

(26) Cooke, H. A., and Bruner, S. D. (2010) Probing the active site of MIO-dependent aminomutases, key catalysts in the biosynthesis of *β*-amino acids incorporated in secondary metabolites. *Biopolymers 93*, 802−810.

(27) Montavon, T. J., Christianson, C. V., Festin, G. M., Shen, B., and Bruner, S. D. (2008) Design and characterization of mechanism-based inhibitors for the tyrosine aminomutase *Sg*TAM. *Bioorg. Med. Chem. Lett. 18*, 3099−3102.

(28) Calabrese, J. C., Jordan, D. B., Boodhoo, A., Sariaslani, S., and Vannelli, T. (2004) Crystal structure of phenylalanine ammonia lyase: Multiple helix dipoles implicated in catalysis. *Biochemistry 43*, 11403−11416.

(29) Schwede, T. F., Retey, J., and Schulz, G. E. (1999) Crystal structure of histidine ammonia-lyase revealing a novel polypeptide modification as the catalytic electrophile. *Biochemistry 38*, 5355−5361.
(30) Louie, G. V., Bowman, M. E., Moffitt, M. C., Baiga, T. J., Moore, B. S., and Noel, J. P. (2006) Structural determinants and modulation of substrate specificity in phenylalanine-tyrosine ammonia-lyases. *Chem. Biol. 13*, 1327−1338.
(31) Rother, D., Poppe, L., Viergutz, S., Langer, B., and Retey, J. (2001) Characterization of the active site of histidine ammonia-lyase from *Pseudomonas putida*. *Eur. J. Biochem. 268*, 6011−6019.
(32) Rother, D., Poppe, L., Morlock, G., Viergutz, S., and Retey, J. (2002) An active site homology model of phenylalanine ammonia-lyase from *Petroselinum crispum*. *Eur. J. Biochem. 269*, 3065−3075.
(33) Schroeder, A. C., Kumaran, S., Hicks, L. M., Cahoon, R. E., Halls, C., Yu, O., and Jez, J. M. (2008) Contributions of conserved serine and tyrosine residues to catalysis, ligand binding, and cofactor processing in the active site of tyrosine ammonia lyase. *Phytochemistry 69*, 1496−1506.
(34) Bartsch, S., Wybenga, G. G., Jansen, M., Heberling, M. M., Wu, B., Dijkstra, B. W., and Janssen, D. B. (2013) Redesign of a phenylalanine aminomutase into a phenylalanine ammonia lyase. *ChemCatChem 5*, 1797−1802.
(35) Givot, I. L., Smith, T. A., and Abeles, R. H. (1969) Studies on the mechanism of action and the structure of the electrophilic center of histidine ammonia lyase. *J. Biol. Chem. 244*, 6341−6353.
(36) Mutatu, W., Klettke, K. L., Foster, C., and Walker, K. D. (2007) Unusual mechanism for an aminomutase rearrangement: Retention of configuration at the migration termini. *Biochemistry 46*, 9785−9794.
(37) Wang, K., Hou, Q., and Liu, Y. (2013) Insight into the mechanism of aminomutase reaction: A case study of phenylalanine aminomutase by computational approach. *J. Mol. Graphics Modell. 46*, 65−73.
(38) Baedeker, M., and Schulz, G. E. (2002) Autocatalytic peptide cyclization during chain folding of histidine ammonia-lyase. *Structure 10*, 61−67.
(39) Christianson, C. V., Montavon, T. J., Festin, G. M., Cooke, H. A., Shen, B., and Bruner, S. D. (2007) The mechanism of MIO-based aminomutases in β-amino acid biosynthesis. *J. Am. Chem. Soc. 129*, 15744−15745.
(40) Kabsch, W. (2010) Integration, scaling, space-group assignment and post-refinement. *Acta Crystallogr. D66*, 133−144.
(41) Evans, P. (2006) Scaling and assessment of data quality. *Acta Crystallogr. D62*, 72−82.
(42) Winn, M. D., Ballard, C. C., Cowtan, K. D., Dodson, E. J., Emsley, P., Evans, P. R., Keegan, R. M., Krissinel, E. B., Leslie, A. G., McCoy, A., McNicholas, S. J., Murshudov, G. N., Pannu, N. S., Potterton, E. A., Powell, H. R., Read, R. J., Vagin, A., and Wilson, K. S. (2011) Overview of the CCP4 suite and current developments. *Acta Crystallogr. D67*, 235−242.
(43) McCoy, A. J., Grosse-Kunstleve, R. W., Adams, P. D., Winn, M. D., Storoni, L. C., and Read, R. J. (2007) Phaser crystallographic software. *J. Appl. Crystallogr. 40*, 658−674.
(44) Murshudov, G. N., Skubak, P., Lebedev, A. A., Pannu, N. S., Steiner, R. A., Nicholls, R. A., Winn, M. D., Long, F., and Vagin, A. A. (2011) *REFMAC5* for the refinement of macromolecular crystal structures. *Acta Crystallogr. D67*, 355−367.
(45) Emsley, P., and Cowtan, K. (2004) Coot: Model-building tools for molecular graphics. *Acta Crystallogr. D60*, 2126−2132.
(46) Chen, V. B., Arendall, W. B., III, Headd, J. J., Keedy, D. A., Immormino, R. M., Kapral, G. J., Murray, L. W., Richardson, J. S., and Richardson, D. C. (2010) MolProbity: All-atom structure validation for macromolecular crystallography. *Acta Crystallogr. D66*, 12−21.
(47) Schuttelkopf, A. W., and van Aalten, D. M. (2004) PRODRG: A tool for high-throughput crystallography of protein-ligand complexes. *Acta Crystallogr. D60*, 1355−1363.
(48) Krissinel, E., and Henrick, K. (2007) Inference of macromolecular assemblies from crystalline state. *J. Mol. Biol. 372*, 774−797.
(49) Adams, P. D., Afonine, P. V., Bunkoczi, G., Chen, V. B., Davis, I. W., Echols, N., Headd, J. J., Hung, L. W., Kapral, G. J., Grosse-Kunstleve, R. W., McCoy, A. J., Moriarty, N. W., Oeffner, R., Read, R. J., Richardson, D. C., Richardson, J. S., Terwilliger, T. C., and Zwart, P. H. (2010) PHENIX: A comprehensive python-based system for macromolecular structure solution. *Acta Crystallogr. D66*, 213−221.
(50) Schrödinger, L. (2010) *The PyMOL molecular graphics system*, version 1.2r3pre, Schrödinger, Inc., Portland, OR.
(51) Barondeau, D. P., Putnam, C. D., Kassmann, C. J., Tainer, J. A., and Getzoff, E. D. (2003) Mechanism and energetics of green fluorescent protein chromophore synthesis revealed by trapped intermediate structures. *Proc. Natl. Acad. Sci. U.S.A. 100*, 12111−12116.
(52) Sniegowski, J. A., Lappe, J. W., Patel, H. N., Huffman, H. A., and Wachter, R. M. (2005) Base catalysis of chromophore formation in Arg96 and Glu222 variants of green fluorescent protein. *J. Biol. Chem. 280*, 26248−26255.
(53) Pilbak, S., Farkas, O., and Poppe, L. (2012) Mechanism of the tyrosine ammonia lyase reaction-tandem nucleophilic and electrophilic enhancement by a proton transfer. *Chemistry 18*, 7793−7802.